

Glacial/interglacial instabilities of the Western Boundary Under Current during the last 365 kyr from Sm/Nd ratios of the sedimentary clay-size fractions at ODP site 646 (Labrador Sea)

Nathalie Fagel^{a,*}, Claude Hillaire-Marcel^b

^a URAP Clay and Paleoclimate, Geology Department, ULg, Liège B-4000, Belgium

^b GEOTOP, UQAM, Montréal, Canada

Received 24 May 2005; received in revised form 11 July 2006; accepted 2 August 2006

Abstract

We present 40 Sm–Nd isotope measurements of the clay-size (<2 μm) fractions of sediments from the Southern Greenland rise (ODP-646) that span the last 365 kyr. These data track changes in the relative supply of fine particles carried into the deep Labrador Sea by the Western Boundary Under Current (WBUC) back to the fourth glacial–interglacial cycles. Earlier studies revealed three general sources of particles to the core site: (i) Precambrian crustal material from Canada, Greenland, and/or Scandinavia (*North American Shield* — NAS), (ii) Palaeozoic or younger crustal material from East Greenland, NW Europe, and/or western Scandinavia (*Young Crust* — YC) and (iii) volcanic material from Iceland and the Mid-Atlantic Ridge (MAR). Clay-size fractions from glacial sediments have the lowest Nd isotopic ratios. Supplies of young crustal particles were similar during glacial oxygen isotope stages (OIS) 2, 6, and 10. In contrast the mean volcanic contributions decreased relative to old craton material from OIS 10 to OIS 6 and then from OIS 6 to OIS 2. The glacial OIS 8 interval displays a mean Sm/Nd ratio similar to those of interglacials OIS 1, 5, and 9. Compared with other interglacials, OIS 7 was marked by a higher YC contribution but a similar ~30% MAR supply. The overall NAS contribution dropped by a factor of 2 during each glacial/interglacial transition, with the MAR contribution broadly replacing it during interglacials. To decipher between higher supplies and/or dilution, particle fluxes from each end member were estimated. Glacial NAS fluxes were systematically higher than interglacial fluxes. During the time interval examined, fine particle supplies to the Labrador Sea were strongly controlled by proximal ice-margin erosion and thus echoed the glacial stage intensity. In contrast, the WBUC-carried MAR supplies from the eastern basins did not change significantly throughout the last 365 kyr, except for a marked increase in surface-sediments that suggests unique modern conditions. Distal WBUC-controlled inputs from the Northern and NE North Atlantic seem to have been less variable than proximal supplies linked with glacial erosion rate.

© 2006 Elsevier B.V. All rights reserved.

Keywords: North Atlantic; Sm–Nd isotopes; deep circulation; Late Quaternary; clay fraction

1. Introduction

With an increasing effort in climate–ocean system modelling, documentation on paleoclimate-related changes in the rate of production of the North Atlantic

* Corresponding author. Université de Liège, URAP Clay and Paleoclimate, Geology Department, B18, Allée du 6 Août, B-4000 Liège, Belgium. Tel.: +32 4 366 2209; fax: +32 4 366 2202.

E-mail address: nathalie.fagel@ulg.ac.be (N. Fagel).

Deep Water (NADW) is needed. Most of the authors agree that the overall NADW production decreased during glacial periods (Boyle and Keigwin, 1982; Shackleton et al., 1983; Duplessy et al., 1988; Broecker et al., 1990; Boyle, 1995). However, their estimates range between a total collapse and a significant reduction (e.g., on the order of 35%; Kissel et al., 1997). During glacials, a greater amount of Southern Ocean waters penetrated into the North Atlantic. Moreover the deep convection in the North Atlantic like that present was replaced by a shallower and a more southern convection (e.g., Oppo and Fairbanks, 1987; Bertram et al., 1995; Ganopolski and Rahmstorf, 2001; Rahmstorf and Alley, 2002).

Despite numerous studies on the paleocirculation in the North Atlantic during the Last Glacial cycle (e.g., Ledbetter and Balsam, 1985; Boyle and Keigwin, 1987; Broecker et al., 1990; Samthein et al., 1994; McCave et al., 1995; Samthein and Altenbach, 1995; Moros et al., 1997; Bauch et al., 2000, 2001; Austin and Kroon, 2001; Lassen et al., 2002; Millo et al., 2003; Kösters et al., 2004), a question remains on whether the last climate cycle is representative of the whole Pleistocene, or at least of the time interval characterized by the 100 kyr eccentricity solar forcing (e.g., Berger, 1980). The information on earlier glacial cycles is indeed less abundant although the paleocirculation of those times has been investigated by several authors, notably by Boyle and Keigwin (1982), Bauch (1997), Kissel et al. (1997), Helmke and Bauch (2003), Raymo et al. (2004), Schonfeld et al. (2003), and St. John et al. (2004). The major outcomes from these studies concerning the evolution of NADW throughout the last Pleistocene glacial–interglacial (G/I) cycles are:

- (1) Variations in magnetic anisotropy measurements on a core from the Iceland basin along the Iceland Scotland Overflow Water (ISOW) pathway was related to a variable strength of the water mass during the last 200 kyr, with a $\sim 30\%$ reduction in strength during glacial Oxygen Isotope Stages (OIS) 2, 4, and 6 compared to interglacials 1, 3, and 5 (Kissel et al., 1997).
- (2) Based on planktic foraminifera $\delta^{18}\text{O}$, CaCO_3 contents, and Ice-Rafted Debris (IRD) in sediment cores from the northeast Atlantic and western Nordic seas, Helmke and Bauch (2003) concluded that during the last 500 kyr, OIS 11, 5e, and 1 have been the only intervals characterized by full interglacial conditions, marked mainly by a northward advection of warm Atlantic surface waters into the Nordic and Arctic seas.
- (3) Based on a compilation of fifty-four $\delta^{13}\text{C}$ values from North Atlantic foraminifers, Raymo et al. (2004) concluded that glacial/interglacial fluctuations in intermediate water chemistry were pronounced only during the last 600 kyr and that the relative volumetric production of Labrador Sea Water (LSW) and of NADW through overflows from the Nordic seas did not change significantly for most of the Pleistocene. In contrast, recent interglacials (notably OIS 1, 5, 9, 11) showed a uniform water-column chemistry, lacking a glacial-like depletion in foraminiferal $\delta^{13}\text{C}$ values. Unusual recent open-sea ice conditions in Nordic seas, with enhanced penetration of North Atlantic Water, may be responsible for the anomalously large volumetric flux of Norwegian Sea Overflow Water (NSOW) today (Raymo et al., 2004).

Most paleoceanographic reconstructions of this critical time interval are based on micropaleontological or derived proxies that are sensitive to ocean ventilation and water mixing (e.g., Snowball and Moros, 2003). Sedimentary abiotic components like magnetic properties (e.g., Kissel et al., 1997; Snowball and Moros, 2003), clay mineral assemblages (Bout-Roumazeilles, 1995; Fagel et al., 1997), and radiogenic isotope abundances in clay-size fraction (Bout-Roumazeilles et al., 1998; Fagel et al., 1999, 2004; Frank et al., 2001) have been less intensively used, although they do provide information on the deep currents. Our aim here is to examine the relative contribution of fine particle supplies in the Labrador Sea by the Western Boundary Under Current (WBUC) during the last four glacial/interglacial cycles (G/I). Earlier studies allowed us to characterize potential geographical sources of particles from Nd signatures of clay-size sedimentary fractions (Innocent et al., 1997; Fagel et al., 1999, 2002). Using this approach on cored sediments from the ODP site 646 off southern Greenland, we draw a reconstruction of the past deep circulation changes in the NW Atlantic throughout the last 365 kyr.

2. Material and method

Site 646 (58°12.56'N, 48°22.15'W, water depth: 3460 m) was drilled in the Labrador Sea during Ocean Drilling Programme Leg 105 (Srivastava et al., 1987; Baldauf et al., 1989). Site 646 is located off Greenland on the upper northern flank of the Eirik Ridge sediment drift (Fig. 1). It is located below the high velocity axis of the WBUC that sweeps the lower Greenland slope

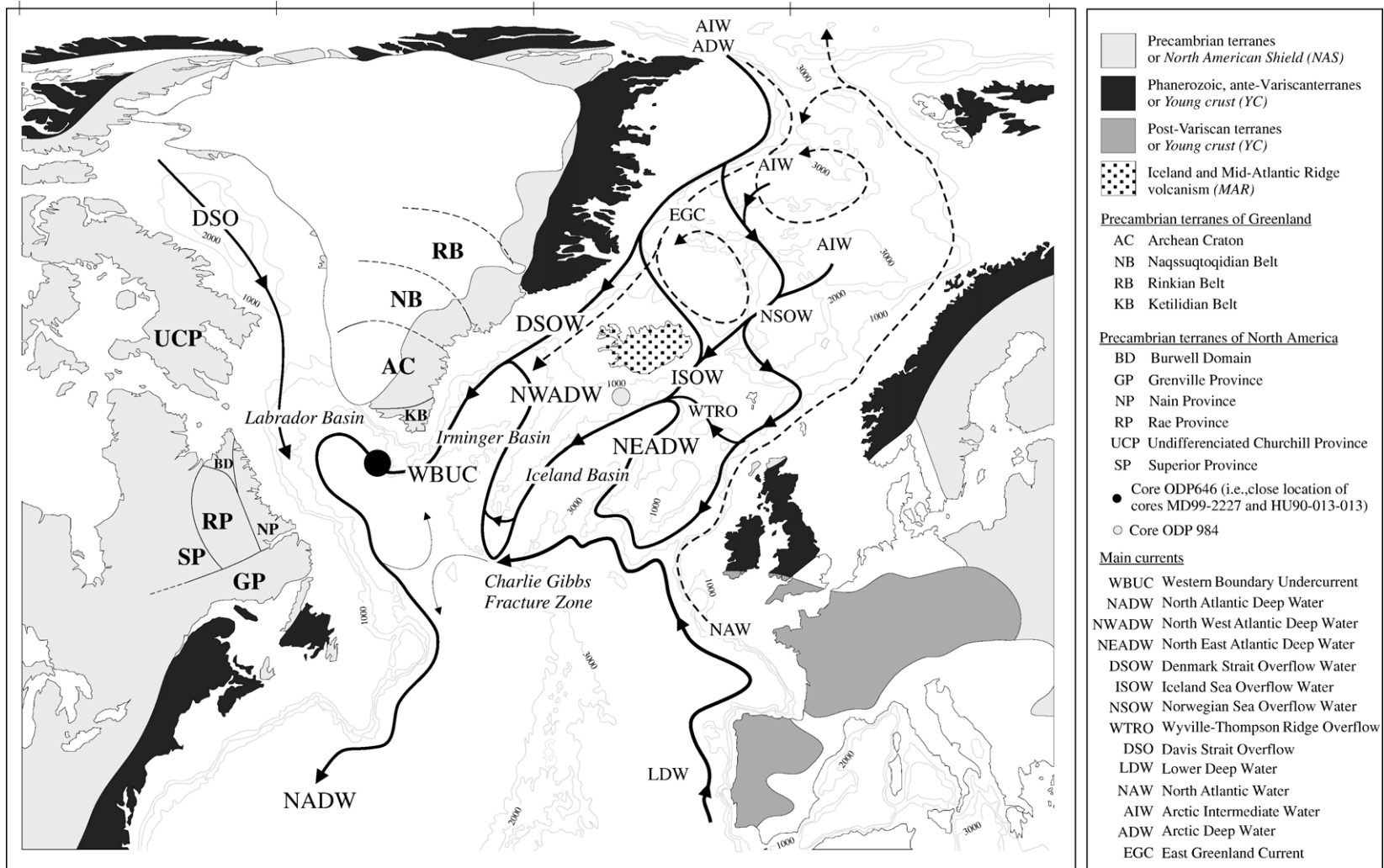


Fig. 1. Location of Site 646, Leg 105 ODP in the Labrador Sea, northern North Atlantic. The plain arrows indicate the pathways of deep or intermediate currents modified from McCartney (1992), Schmitz and Mc Cartney (1993), Dickson and Brown (1994), Lucotte and Hillaire-Marcel (1994) and Hansen and Osterhus (2000). The broken arrows indicate surface circulation adapted from Hansen and Osterhus (2000). The structural terranes of the continental crust adjacent to the northern North Atlantic are schematically indicated by different shades of grey and Iceland volcanism by dots (Fagel et al., 2004).

(McCartney, 1992; Schmitz and Mc Cartney, 1993; Lucotte and Hillaire-Marcel, 1994). The WBUC drives NADW components overflowing the Denmark-Iceland-Faroe-Shetland sills [i.e., the Norwegian Sea Overflow Water (NSOW), the Iceland Sea Overflow Water (ISOW), and the Denmark Strait Overflow Water (DSOW)] as well as a recirculated fraction of the Davis Strait Overflow, into a deep gyre in the Labrador Sea (McCartney, 1992; Schmitz and Mc Cartney, 1993; Dickson and Brown, 1994; Hansen and Osterhus, 2000). The Labrador Sea Water (LSW) occupies the water column above NADW water masses: its lower boundary ranges from 1100 m on Greenland slope to 2000 m in the basin. Surface waters are under the subpolar West Greenland Current (WGC) influence.

Two cores, 646A (water depth 3462 m) and 646B (water depth 3459 m), were combined into a composite section, using lithostratigraphic and magnetic correlations (Srivastava et al., 1987). A complete upper Pleistocene and Holocene section, spanning from OIS 27 to 1, is represented in the upper 78 m of sediments. The chronostratigraphy is based on oxygen-isotope measurements in planktonic foraminifers (Fig. 2) combined with magnetostratigraphy and biostratigraphy (Aksu et al., 1989; Baldauf et al., 1989). Sediments at Site 646 consist primarily of clayey and silty muds, with variable amounts (5–20% or more) of biogenic and detrital carbonates. In contrast, the upper 150 cm

corresponding to OIS 1 is composed of a muddy foraminiferal ooze (Baldauf et al., 1989). In the underlying sediments, thin (<1 cm) white detrital carbonate-rich sandy layers are interpreted as deposited from turbidity currents that breached the levees of the North Atlantic Mid-Ocean Canyon (NAMOC; Hiscott et al., 1989). Sandy and gravely material is scattered or occasionally concentrated in layers in the hemipelagic muddy sediment. They represent up to 15% by weight of the sediment and are interpreted as Ice-Rafted Detritus (IRD; Asku et al., 1992).

Here, we analyzed the <2 μm size fraction, i.e., the sediment fraction that is least affected by ice rafting and consequently more representative of the suspended particulate load of deep currents (Fagel et al., 2002). Subsampling was at 20 cm intervals (173 samples) in the upper 32 m of the composite sequence (henceforth, all depths corresponds to composite-core depths). This sediment section spans from the OIS 10 to OIS 1 time interval. Sedimentation rates ranged between 5 and 15 cm/kyr throughout this interval (Hillaire-Marcel et al., 1990), with a mean of 8 cm/kyr (Baldauf et al., 1989). The sampling interval allows a mean time resolution of 2500 yr. An age model has been set using magnetic susceptibility data measured on ODP 646 core (Baldauf et al., 1989; F. Hall, unpublished data) and correlations with magnetic data sets from two other cores (MD99-2227 and HU90-013-013) from nearby

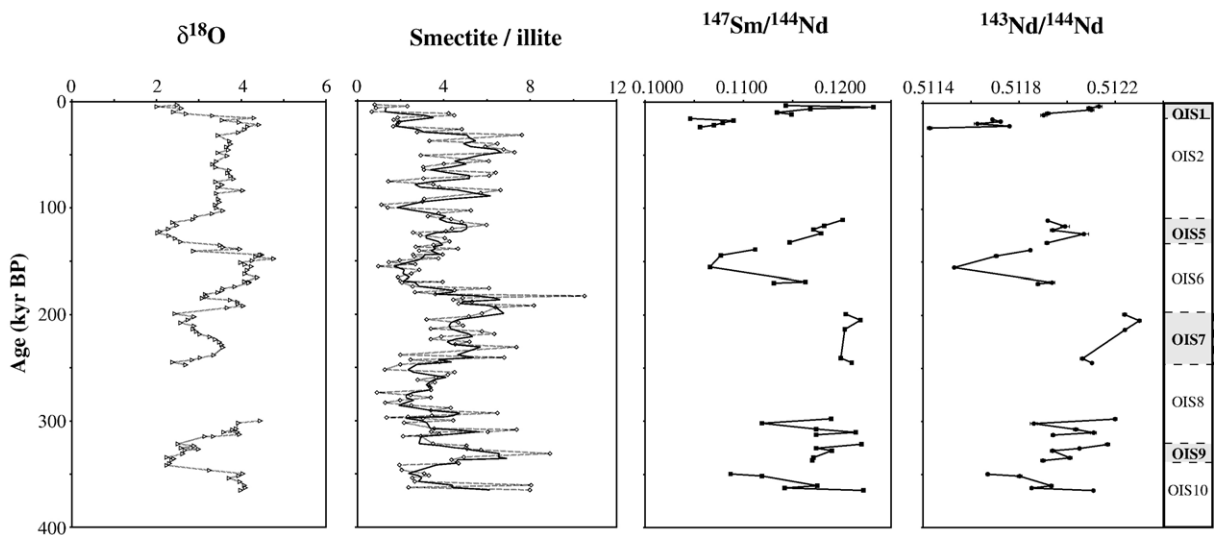


Fig. 2. Oxygen isotope stratigraphy, smectite/illite ratios and Sm and Nd isotopic data of the clay-size fraction reported versus age model, Site 646 Leg 105 ODP. The clay mineral variability is summarized by the relative abundance of smectite and illite (data from Table 1). The 20 cm-sampling interval allows for an averaged resolution of 2500 years for clay mineralogy. Individual clay data points were smoothed with a 3-point moving average (bold curve). The interglacial/glacial stage numbers or Oxygen Isotope Stage (OIS) are reported according to the oxygen isotope stratigraphy on the right side of the diagram. Five samples have been selected in each OIS for Sm/Nd and Nd/Nd analyses. The accuracy on $^{147}\text{Sm}/^{144}\text{Nd}$ ratios is better than 2%. Error bars on $^{143}\text{Nd}/^{144}\text{Nd}$ ratios are indicated when higher than symbols used (data from Table 1).

Table 1

Clay mineralogical assemblages, Sm–Nd concentrations, Sm and Nd isotopic ratios reported in regard with the oxygen isotope ratios, the corresponding OIS number and the estimated age model

| Stratigraphy ODP646 | | | | Clay mineralogy | | | | | Sm–Nd signature of the clay fraction | | | | | | Contribution | | | Estimated flux | | | | |
|---------------------|--------------|-----------------------|-------|-----------------|-------|--------|-------|-----|--------------------------------------|------------|-----------------------------------|-----------------------------------|------------------------|-------------------------|--------------|--------|---------|---|------------------|-----------------|------------------|--|
| Depth (cm) | Age (kyr BP) | $\delta^{18}\text{O}$ | O.I.S | C (%) | I (%) | Sm (%) | K (%) | S/I | [Nd] (ppm) | [Sm] (ppm) | $^{147}\text{Sm}/^{144}\text{Nd}$ | $^{143}\text{Nd}/^{144}\text{Nd}$ | ϵ_{Nd} | 2σ (10^{-6}) | NAS (%) | YC (%) | MAR (%) | Clay flux ($\text{g}/\text{cm}^2/\text{kyr}$) | NAS ^a | YC ^a | MAR ^a | |
| 40 | 3.2 | 2.5 | 1 | 21 | 36 | 28 | 15 | 0.8 | 16 | 3.1 | 0.1143 | 0.512132 | -9.9 | 13 | 0 | 100 | 0 | 0.5 | 0.0 | 0.9 | 0.0 | |
| 60 | 4.8 | 2.0 | 1 | 13 | 23 | 54 | 10 | 2.3 | 30 | 6.0 | 0.1232 | 0.512091 | -10.7 | 9 | 15 | 50 | 35 | 0.3 | 0.2 | 0.2 | 0.1 | |
| 80 | 6.4 | 2.6 | 1 | 21 | 33 | 30 | 16 | 0.9 | 20 | 3.9 | 0.1168 | 0.512100 | -10.5 | 11 | 0 | 90 | 10 | 0.3 | 0.0 | 0.4 | 0.0 | |
| 120 | 9.8 | 2.4 | 1 | 16 | 42 | 29 | 13 | 0.7 | 20 | 3.7 | 0.1134 | 0.511919 | -14.0 | 10 | 20 | 70 | 10 | 0.7 | 0.5 | 0.7 | 0.1 | |
| 140 | 12.6 | 2.7 | 1 | 12 | 15 | 62 | 11 | 4.2 | 21 | 4.0 | 0.1149 | 0.511902 | -14.4 | 13 | 25 | 60 | 15 | 0.7 | 0.7 | 0.7 | 0.1 | |
| 180 | 15.5 | 4.3 | 2 | 17 | 25 | 46 | 12 | 1.9 | 26 | 4.5 | 0.1046 | 0.511689 | -18.5 | 6 | 45 | 55 | 0 | 2.1 | 3.8 | 1.8 | 0.0 | |
| 200 | 17.5 | 3.6 | 2 | 15 | 27 | 46 | 12 | 1.7 | 33 | 5.8 | 0.1090 | 0.511723 | -17.8 | 5 | 40 | 55 | 5 | 1.5 | 2.5 | 1.3 | 0.1 | |
| 220 | 19.5 | 4.0 | 2 | 14 | 25 | 48 | 13 | 1.9 | 29 | 5.1 | 0.1079 | 0.511627 | -19.7 | 14 | 50 | 40 | 10 | 1.7 | 3.5 | 1.1 | 0.2 | |
| 240 | 21.8 | 4.4 | 2 | 15 | 26 | 47 | 12 | 1.8 | 33 | 5.8 | 0.1070 | 0.511760 | -17.1 | 5 | 40 | 60 | 0 | 1.9 | 3.2 | 1.8 | 0.0 | |
| 260 | 23.6 | 4.2 | 2 | 16 | 27 | 45 | 12 | 1.7 | 36 | 6.2 | 0.1056 | 0.511428 | -23.6 | 10 | 70 | 15 | 15 | 1.0 | 2.9 | 0.2 | 0.2 | |
| 900 | 110.9 | 2.9 | 5 | 9 | 15 | 68 | 8 | 4.3 | 34 | 6.7 | 0.1201 | 0.511919 | -14.0 | 4 | 30 | 35 | 35 | 0.6 | 0.8 | 0.3 | 0.3 | |
| 940 | 116.4 | 2.5 | 5 | 9 | 12 | 70 | 9 | 6.0 | 32 | 6.3 | 0.1182 | 0.511991 | -12.6 | 19 | 20 | 55 | 25 | 0.5 | 0.4 | 0.5 | 0.2 | |
| 960 | 119.9 | 2.3 | 5 | 11 | 15 | 64 | 10 | 4.4 | 30 | 5.8 | 0.1171 | 0.511940 | -13.6 | 10 | 25 | 50 | 25 | 0.4 | 0.5 | 0.3 | 0.2 | |
| 1000 | 123.5 | 2.0 | 5 | 11 | 22 | 55 | 12 | 2.6 | 29 | 5.5 | 0.1179 | 0.512069 | -11.1 | 20 | 10 | 75 | 15 | 0.2 | 0.1 | 0.2 | 0.0 | |
| 1060 | 131.5 | 2.6 | 5 | 10 | 15 | 65 | 10 | 4.3 | 28 | 5.2 | 0.1147 | 0.511916 | -14.1 | 9 | 25 | 60 | 15 | 1.1 | 1.1 | 1.0 | 0.2 | |
| 1140 | 138.7 | 4.0 | 6 | 10 | 14 | 67 | 9 | 4.7 | 29 | 5.3 | 0.1112 | 0.511847 | -15.4 | 5 | 25 | 70 | 5 | 1.1 | 1.2 | 1.2 | 0.1 | |
| 1200 | 144.2 | 4.4 | 6 | 9 | 23 | 58 | 10 | 2.6 | 36 | 6.3 | 0.1077 | 0.511705 | -18.2 | 9 | 45 | 55 | 0 | 1.2 | 2.2 | 1.0 | 0.0 | |
| 1320 | 155.1 | 4.2 | 6 | 15 | 38 | 37 | 10 | 1.0 | 36 | 6.3 | 0.1066 | 0.511530 | -21.6 | 4 | 60 | 30 | 10 | 1.3 | 3.2 | 0.6 | 0.2 | |
| 1400 | 169.0 | 4.1 | 6 | 7 | 29 | 58 | 6 | 2.0 | 32 | 6.1 | 0.1163 | 0.511937 | -13.7 | 11 | 25 | 55 | 20 | 1.2 | 1.3 | 1.0 | 0.3 | |
| 1440 | 170.1 | 4.2 | 6 | 13 | 24 | 50 | 13 | 2.1 | 32 | 5.9 | 0.1131 | 0.511878 | -14.8 | 8 | 20 | 70 | 10 | 1.5 | 1.3 | 1.7 | 0.2 | |
| 1720 | 199.1 | 2.4 | 7 | 10 | 12 | 72 | 6 | 5.8 | 30 | 6.0 | 0.1204 | 0.512239 | -7.8 | 9 | 0 | 80 | 20 | 1.5 | 0.0 | 1.8 | 0.4 | |
| 1760 | 204.8 | 2.7 | 7 | 13 | 19 | 60 | 8 | 3.2 | 26 | 5.3 | 0.1219 | 0.512300 | -6.6 | 8 | 0 | 75 | 25 | 1.1 | 0.0 | 1.3 | 0.4 | |
| 1820 | 213.5 | | 7 | 13 | 17 | 60 | 10 | 3.4 | 27 | 5.4 | 0.1203 | 0.512240 | -7.8 | 5 | 0 | 80 | 20 | 0.9 | 0.0 | 1.1 | 0.3 | |
| 2040 | 240.6 | 3.0 | 7 | 6 | 12 | 78 | 4 | 6.8 | 26 | 5.2 | 0.1199 | 0.512064 | -11.2 | 10 | 15 | 60 | 25 | 0.9 | 0.6 | 0.9 | 0.3 | |
| 2080 | 244.8 | 2.4 | 7 | 12 | 16 | 63 | 9 | 3.8 | 33 | 6.6 | 0.1210 | 0.512103 | -10.4 | 6 | 10 | 65 | 25 | 1.0 | 0.4 | 1.0 | 0.3 | |
| 2520 | 297.7 | 4.5 | 8 | 10 | 15 | 68 | 7 | 4.4 | 28 | 5.5 | 0.1189 | 0.512199 | -8.6 | 8 | 0 | 85 | 15 | 1.5 | 0.0 | 2.0 | 0.3 | |
| 2560 | 301.9 | 3.9 | 8 | 11 | 25 | 53 | 11 | 2.2 | 30 | 5.4 | 0.1119 | 0.511861 | -15.2 | 14 | 25 | 70 | 5 | 1.7 | 1.7 | 1.8 | 0.1 | |
| 2580 | 307.3 | 3.9 | 8 | 8 | 19 | 65 | 8 | 3.6 | 29 | 5.6 | 0.1174 | 0.512036 | -11.8 | 10 | 15 | 70 | 15 | 1.6 | 1.0 | 1.8 | 0.3 | |
| 2640 | 310.4 | 3.9 | 8 | 11 | 19 | 63 | 7 | 3.4 | 32 | 6.3 | 0.1214 | 0.512110 | -10.3 | 12 | 10 | 65 | 25 | 1.6 | 0.7 | 1.6 | 0.6 | |
| 2660 | 312.3 | 4.0 | 8 | 8 | 18 | 67 | 7 | 3.8 | 40 | 7.6 | 0.1174 | 0.511941 | -13.6 | 8 | 25 | 50 | 25 | 1.3 | 1.4 | 1.0 | 0.5 | |
| 2760 | 321.6 | 2.5 | 9 | 11 | 18 | 65 | 6 | 3.5 | 29 | 5.9 | 0.1220 | 0.512168 | -9.2 | 10 | 5 | 70 | 25 | 0.9 | 0.2 | 1.0 | 0.3 | |
| 2800 | 325.4 | 2.6 | 9 | 12 | 13 | 67 | 8 | 5.0 | 23 | 4.5 | 0.1174 | 0.512051 | -11.5 | 5 | 10 | 75 | 15 | 0.5 | 0.2 | 0.6 | 0.1 | |
| 2840 | 327.6 | 2.7 | 9 | 8 | 13 | 71 | 8 | 5.7 | 30 | 5.9 | 0.1190 | 0.511939 | -13.6 | 10 | 30 | 40 | 30 | 0.2 | 0.3 | 0.1 | 0.1 | |
| 2880 | 334.2 | 2.2 | 9 | 9 | 14 | 69 | 8 | 4.9 | 30 | 5.8 | 0.1171 | 0.512011 | -12.2 | 9 | 15 | 70 | 15 | 0.7 | 0.5 | 0.8 | 0.2 | |
| 2920 | 336.8 | 2.4 | 9 | 9 | 16 | 67 | 8 | 4.4 | 32 | 6.1 | 0.1170 | 0.511899 | -14.4 | 9 | 30 | 45 | 25 | 0.6 | 0.7 | 0.4 | 0.2 | |
| 3000 | 349.6 | 4.0 | 10 | 14 | 19 | 57 | 10 | 3.1 | 28 | 5.0 | 0.1087 | 0.511669 | -18.9 | 7 | 45 | 45 | 10 | 1.0 | 1.8 | 0.7 | 0.1 | |
| 3020 | 351.5 | 3.9 | 10 | 12 | 18 | 61 | 9 | 3.3 | 31 | 5.8 | 0.1119 | 0.511802 | -16.3 | 10 | 35 | 55 | 10 | 1.2 | 1.7 | 1.0 | 0.2 | |
| 3100 | 360.6 | 4.1 | 10 | 6 | 10 | 79 | 5 | 8.0 | 29 | 5.6 | 0.1175 | 0.511934 | -13.7 | 8 | 25 | 50 | 25 | 1.3 | 1.3 | 1.0 | 0.4 | |
| 3120 | 362.7 | 4.1 | 10 | 15 | 22 | 53 | 10 | 2.4 | 33 | 6.2 | 0.1142 | 0.511852 | -15.3 | 7 | 35 | 50 | 15 | 1.0 | 1.5 | 0.8 | 0.2 | |
| 3140 | 365.1 | 4.0 | 10 | 9 | 9 | 73 | 9 | 8.0 | 29 | 5.9 | 0.1222 | 0.512109 | -10.3 | 5 | 10 | 60 | 30 | 1.1 | 0.5 | 1.0 | 0.5 | |
| Mean ODP646 | | | | 11.78 | 20.25 | 58.45 | 9.53 | 3.5 | 29 | 5.6 | 0.1154 | 0.511941 | -13.6 | 9 | | | | | | | | |

NAS, North American Shield; YC, Young crust; MAR, Mid-Atlantic Ridge volcanism; C, chlorite; I, illite; Sm, smectite; K, kaolinite.

Note the % corresponds to the relative abundance of each clay species within the clay–mineral fraction summed to 100%.

^a Normalized flux, i.e., measured clay flux divided by the present flux measured in surface sediment 90-013-017 sample.

sites (J. Stoner, unpublished data; Stoner et al., 1998). This age model allowed us to assign a tentative age to each sample for the 365 kyr interval (Table 1).

Clay mineralogy was determined by X-ray diffraction on the carbonate-free $<2 \mu\text{m}$ fraction, using a method detailed in Fagel et al. (1997). Briefly, the samples were sieved under water at $63 \mu\text{m}$. The silt fraction was then decalcified in 0.1 N HCl to avoid any Rare Earth Element leaching (Innocent et al., 1999). After removing excess acid by repeated washings, the $<2 \mu\text{m}$ clay-size fraction was separated after settling according to Stoke's law. Oriented mounts were made using the glass slide method (Moore and Reynolds, 1989) then analysed on a Siemens X-ray diffractometer with $\text{CoK}\alpha$ radiation (GEOTOP, UQAM). Semi-quantitative estimates ($\pm 5\%$ within the whole clay assemblages) of the most abundant clay minerals were based on the area of their diffraction peaks measured on the ethylene-glycol scan. Estimations based on peak areas allow us to minimize errors related to crystallinity changes of the samples (Fagel et al., 1997). In order to normalize the data, the area of the 17 \AA peak was divided by the area of the 10 \AA peak to calculate a smectite/illite ratio.

Sm–Nd isotopic signatures were determined in forty samples selected as follows: 5 samples from each interglacial (i.e., OIS 1, 5, 7, 9) and glacial intervals (i.e., OIS 2, 6, 8, 10) with some of them representing deglacial transitions. Sm–Nd concentrations and isotopic ratios were measured on the

carbonate-free clay-size fraction ($<2 \mu\text{m}$). The abundance of this clay-size fraction, estimated by weighting after three successive settlings, represents less than 8% of the bulk sediments. It is slightly but systematically higher in glacials [mean = $6\% \pm 0.9$ (1σ standard deviation)] than in interglacials [mean = $3.7\% \pm 1.4$ (1σ standard deviation)]. Sm–Nd data were obtained using a VG-Thermal Ionisation Mass Spectrometer from the GEOTOP research Centre. Sm–Nd were loaded on a double Re-Ta filament, then run in static or dynamic multicollection mode, respectively. The accuracy of the isotopic analyses was controlled by running La Jolla standard: the average value of 21 analyses was 0.511849 ± 12 (2σ standard deviation). Blanks were considered negligible for both Sm and Nd: lower than 150 pg for the whole procedure. For the full analytical procedure, see Innocent et al. (1997).

3. Results: Mineralogical and Sm/Nd isotopic signature of the clay-size fraction

In all samples the carbonate-free $<2 \mu\text{m}$ fraction comprises clays minerals, quartz, feldspars and amphibole. On average, clay assemblages include $\sim 60\%$ smectites, $\sim 20\%$ illite, and $\sim 10\%$ each chlorite and kaolinite (Table 1). Changes are observed between glacials and interglacials. Glacials show a marked drop in smectite content (down to 40%) and a corresponding increase in illite and chlorite. Interglacials show an

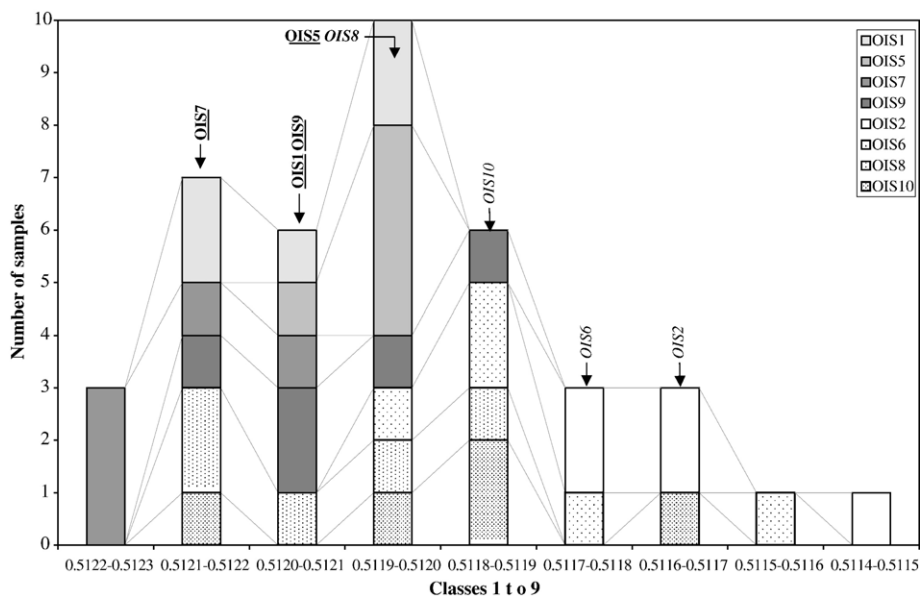


Fig. 3. Distribution of the $^{143}\text{Nd}/^{144}\text{Nd}$ ratios measured on the clay-size fraction. Nd data have been split within 9 classes corresponding to a range of variation of 0.0001. Arrows indicate mean values for 6 of the OIS. Data from Table 1, means from Table 2.

increase in the smectite content, except OIS 1, which shows the lowest smectite content (40%). The clay mineral variability is expressed by the relative abundance of smectite and illite and it is defined by a smectite/illite ratio (S/I) directly measured on the ethylene-glycol solvated scan (Fig. 2).

$^{143}\text{Nd}/^{144}\text{Nd}$ ratios of the $<2\ \mu\text{m}$ fraction vary between 0.51143 ($\epsilon\text{Nd}=-24$) and 0.51230 ($\epsilon\text{Nd}=-7$), whereas $^{147}\text{Sm}/^{144}\text{Nd}$ ratios range from 0.1056 to 0.1232 (Table 1). As shown in Fig. 3, Nd data show a higher scatter during glacial stages (from 0.51220 to 0.51143, i.e., up to 15 ϵNd units) than during interglacials (from 0.51217 to 0.51190, a range ≤ 8 ϵNd units; Fig. 3). The larger scatter in glacial intervals is due to the occurrence of a few samples with low (unradiogenic) Nd isotope ratios. Glacial stages are thus characterized by overall lower Nd ratios (i.e., *unradiogenic* compositions with a mean $\epsilon\text{Nd}=-15.7\pm 0.2$; Table 2) than interglacial stages (mean $\epsilon\text{Nd}=-11.5\pm 0.2$; Table 2). The highest Nd isotope ratios are seen in the interglacial stage OIS 7 unit, whereas OIS 2 clay-size fractions show the lowest Nd isotope ratios (Table 1). When plotted in a $^{143}\text{Nd}/^{144}\text{Nd}$ versus $^{147}\text{Sm}/^{144}\text{Nd}$ diagram (Fig. 4a), all the mean Sm–Nd values of OIS stages show a positive linear regression trend ($r^2=0.94$). As illustrated above, the mean OIS 7 shows the highest isotopic ratio of the sequence, with a mean Nd isotopic composition similar to that of the surface sediment data point (but with a significantly lower $^{147}\text{Sm}/^{144}\text{Nd}$ ratio). The three other interglacial stages (i.e., OIS 1, 5, and 9) cluster close to glacial OIS 8 values.

Mean values obtained for two nearby cores are in agreement with those obtained here. In core MD99-

2227 (58°12.64'N, 48°22.38'W, 3460 m of water depth), the mean OIS 1 value is close to interglacial compositions measured here, this is especially true for samples older than 6 kyr. In core HU90-013-013 (58°12.59'N, 48°22.40'W, North of Eirik Ridge, 3380 m of water depth), all the data plot along a parallel regression line, slightly shifted towards higher $^{147}\text{Sm}/^{144}\text{Nd}$ ratios, when compared to data from site 646 (Fig. 4a).

4. Discussion and interpretation

4.1. Characterization of Sm–Nd particulate sources

In marine sediments, Sm and Nd are supplied from oceanic volcanism and subaerial erosion (Goldstein and O'Nions, 1981; Goldstein and Jacobsen, 1987). They are mainly carried by river systems and dispersed by oceanic currents (Dia et al., 1992; Revel et al., 1996) or airborne transport (Grousset et al., 1988). Innocent et al. (1997) and Fagel et al. (1999) compiled published Sm–Nd data for potential geological sources of Nd to the Labrador Sea. Briefly, these can be grouped into three categories: (1) a mantle source from the mid-Atlantic oceanic volcanism grouping Iceland, the Faeroe Islands and Reykjanes Ridge (i.e., from the Mid-Atlantic Ridge, abridged henceforth “MAR” end member); (2) Palaeozoic or Younger Crustal (YC) material from NW Europe, W Scandinavia, and NE Greenland; (3) old Precambrian crustal material from Scandinavia, Greenland, and Canada (“NAS” for North-American Shield). The old crustal material is the most widely distributed of the end members. Sm–Nd data at Site

Table 2
Mean values calculated for individual stages and for all the interglacial and glacial stages

| Depth interval (cm) | Age (kyr BP) | O.I.S. | SR (cm/kyr) | $<2\ \mu\text{m}$ (%) | Clay flux ($\text{g}/\text{cm}^2/\text{kyr}$) | S/I | [Nd] (ppm) | [Sm] (ppm) | $^{147}\text{Sm}/^{144}\text{Nd}$ | $^{143}\text{Nd}/^{144}\text{Nd}$ | 2σ (10^{-6}) | ϵ_{Nd} |
|--------------------------|--------------|--------|-------------|-----------------------|---|-----|------------|------------|-----------------------------------|-----------------------------------|-------------------------|------------------------|
| 0 | 0 | 1 | 14 | 5 | 1.6 (1 ^a) | 0.8 | 38 | 8 | 0.1288 | 0.512193 | 20 | -8.7 |
| 40–140 | 3–10 | 1 | 12.4 | 2 | 0.3 ^a | 1.8 | 21 | 4.1 | 0.1165 | 0.512029 | 15 | -11.9 |
| 180–260 | 15–24 | 2 | 11.2 | 6 | 1 ^a | 1.8 | 31 | 5.5 | 0.1068 | 0.511645 | 9 | -19.3 |
| 900–1060 | 82–102 | 5 | 7.4 | 3 | 0.4 ^a | 4.3 | 31 | 5.9 | 0.1176 | 0.511967 | 7 | -13.1 |
| 1140–1440 | 138–170 | 6 | 10.1 | 5 | 0.8 ^a | 2.5 | 33 | 6.0 | 0.1110 | 0.511779 | 6 | -16.7 |
| 1720–2080 | 199–245 | 7 | 9.9 | 5 | 0.7 ^a | 4.6 | 29 | 5.7 | 0.1207 | 0.512189 | 7 | -8.8 |
| 2520–2660 | 298–310 | 8 | 10.6 | 6 | 1 ^a | 3.5 | 32 | 6.1 | 0.1174 | 0.512029 | 10 | -11.9 |
| 2760–2920 | 322–337 | 9 | 8.8 | 3 | 0.4 ^a | 4.7 | 29 | 5.6 | 0.1185 | 0.512014 | 8 | -12.2 |
| 3000–3140 | 350–365 | 10 | 8.4 | 6 | 0.7 ^a | 5.0 | 30 | 5.7 | 0.1149 | 0.511873 | 7 | -15 |
| Mean glacial stages | | | | | | 3.2 | 31 | 5.8 | 0.1125 | 0.511832 | | -15.7 |
| Mean interglacial stages | | | | | | 3.8 | 27 | 5.3 | 0.1183 | 0.512050 | | -11.5 |

O.I.S., oxygen isotope stage; SR, sedimentation rate.

^a Normalized flux, i.e., measured clay flux divided by the present flux measured in surface sediment 90-013-017 sample.

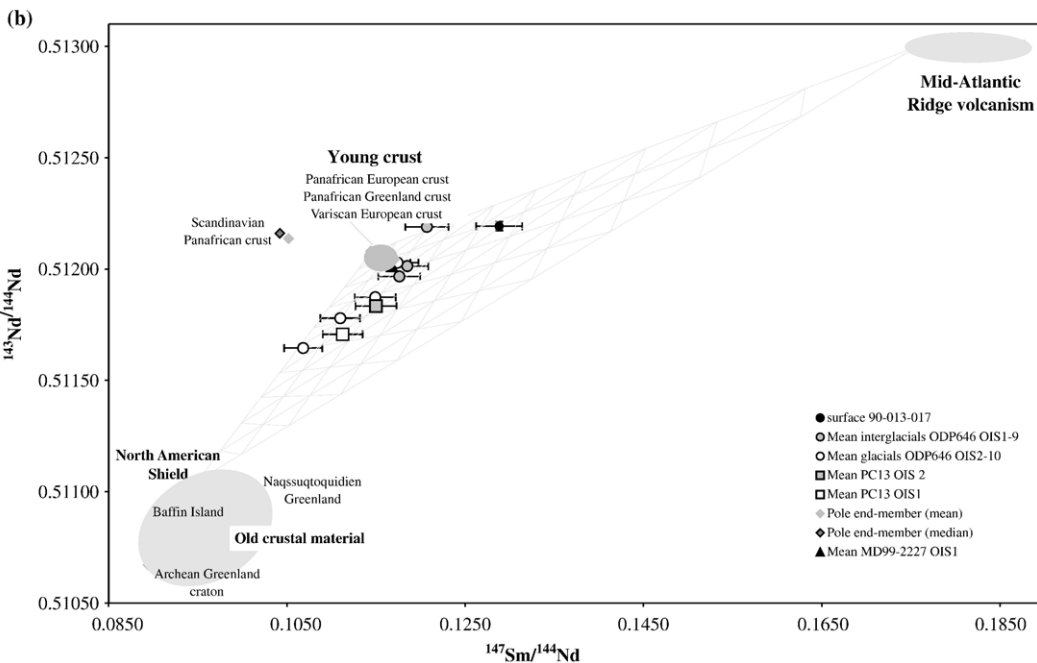
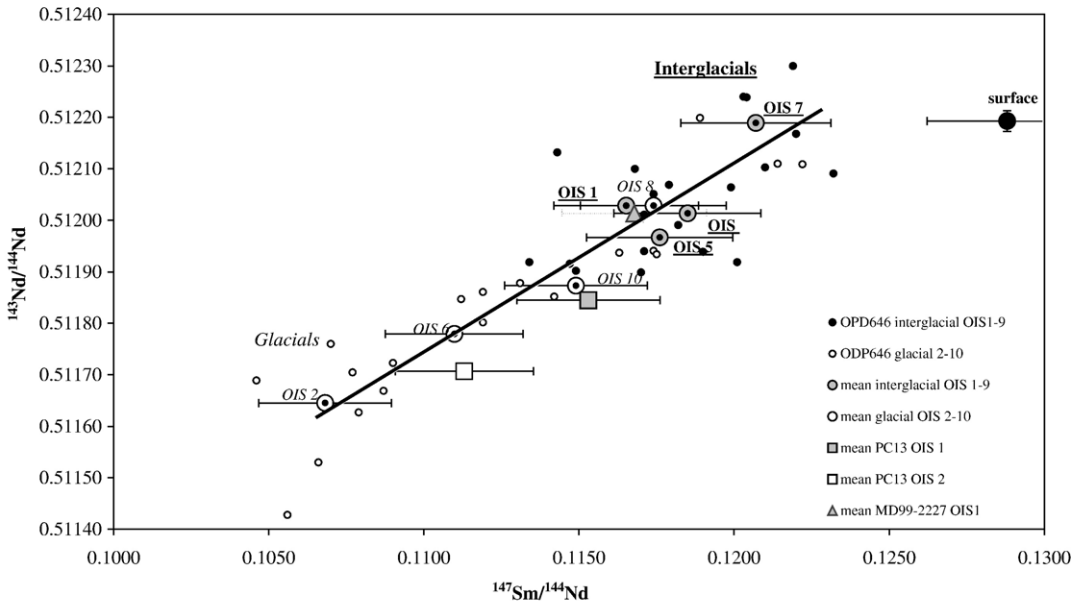
646 (Fig. 4b) suggest that the fine sediments represent variable mixtures of these three sources during glacials and interglacials.

We calculated a mixing grid based on different proportions of the three end members using a standard Sm–Nd mixing pattern (Fig. 4b): the three variables are the $^{147}\text{Sm}/^{144}\text{Nd}$ ratio, the $^{143}\text{Nd}/^{144}\text{Nd}$ ratio, and the Nd content of each end member. Sm content is

calculated from the Nd content and the $^{147}\text{Sm}/^{144}\text{Nd}$ ratio. We calculate for each grid point, the overall Nd and the Sm isotope signature taking into account variable contributions (α) of the three end-members, as follows (Faure, 1986):

$$(i) \quad ^{143}\text{Nd}/^{144}\text{Nd}_{\text{ratio}_{\text{mix}}} = \alpha_1[\text{Nd}]_1(^{143}\text{Nd}/^{144}\text{Nd})_1 + \alpha_2[\text{Nd}]_2(^{143}\text{Nd}/^{144}\text{Nd})_2 + \alpha_3[\text{Nd}]_3(^{143}\text{Nd}/^{144}\text{Nd})_3$$

(a) Sm-Nd data of the clay < 2µm fraction, Greenland Rise (Labrador Sea)



- (ii) $^{147}\text{Sm}/^{144}\text{Nd} \text{ ratio}_{\text{mix}} = ([\text{Sm}]_{\text{mix}}/[\text{Nd}]_{\text{mix}}) \times 0.60847$
 (iii) $\alpha_1 + \alpha_2 + \alpha_3 = 1$.

4.2. Evolution of Sm/Nd supplies during the last 365 kyr

The mean Sm/Nd ratios of glacial intervals OIS 2, 6, and 10 lay along a mixing line parallel to the NAS-MAR axis within the mixing grid. The supplies from young crustal Sm/Nd sources remained more or less constant (~40%) among these three glacial intervals, whereas the mean volcanic contribution decreased, relatively to old craton material, from OIS 6 to OIS 2 and from OIS 10 to OIS 6 (Fig. 4b). The glacial OIS 8 interval displays a mean Sm/Nd ratio similar to those of the interglacials OIS1, 5, and 9. In contrast, the mean OIS 7 value plots along the YC-MAR axis. Its high YC contribution is distinct but it nonetheless contains a ~30% MAR fraction like all other interglacials (Fig. 4b).

To account for the scattering of Sm/Nd signatures within each OIS (see Fig. 3), we calculated the relative contributions of the three selected end-members NAS, YC, and MAR for each ODP 646 sample (Table 1). These contributions are estimated from the 10%-increment mixing grid of Fig. 4b. There is no gradual deglacial trend, except during OIS 6/5 (where MAR evolved from 0 in late OIS 6 to 40% in the early OIS 5). In addition to internal variations within each OIS (presumably underestimated due to our low sampling resolution), the average relative contribution of NAS dropped by a factor of 2 during deglaciations. Enhanced MAR contributions then replaced the lower relative NAS supplies during interglacials. This relative reduction in NAS supplies could be due to either a decrease of NAS fluxes or

higher fluxes of the others two end members (dilution process), or to both processes.

4.3. Changes in clay-size fluxes during deglaciations

In order to decipher between higher supplies or dilution, we estimate the particle flux supplies from the three end-members:

- (i) $F_{\text{EM1}} = \text{EM1} \times F_{\text{c}}$; $F_{\text{EM2}} = \text{EM2} \times F_{\text{c}}$; $F_{\text{EM3}} = \text{EM3} \times F_{\text{c}}$
 (ii) $F_{\text{c}} = \rho_{\text{c}} \times \text{SR} \times f_{\text{c}}$

where

- F_{EM} = end-member flux in $\text{g}/\text{cm}^2/\text{kyr}$;
- EM = %end-member calculated within the 3 end-member mixing;
- ρ_{c} = clay density in g/cm^3 , estimated at 2.3 for all the samples (Callière et al., 1982);
- SR = sedimentation rate in cm/kyr , interpolated from the age model;
- f_{c} = % <2 μm , i.e. the abundance of clay-size fraction in the sediment sample estimated by weighting after successive (at least three) clay-size extraction from suspended carbonate-free 63 μm fraction; extraction was done after settling time according to the Stokes's law, the abundance of <63 μm fraction was estimated after sieving of an initial known weight of bulk sediment (~3 g).

The mean apparent sedimentation rate varies between 7 and 12 cm/kyr . The clay-size fraction ranges from 2% to 6% of the bulk sediment (Table 2). The total clayey flux thus ranges from 0.2 to 2.1 $\text{g}/\text{cm}^2/\text{kyr}$ (Table 1). Clay-size particle fluxes are systematically higher during glacials than during interglacials, essentially as

Fig. 4. $^{143}\text{Nd}/^{144}\text{Nd}$ versus $^{147}\text{Sm}/^{144}\text{Nd}$ diagram. (a) Sm/Nd isotopic composition of the clay-size fraction measured for 40 samples from Site 646, Leg 105 ODP (circle). Mean value for each OIS is plotted as a larger circle. The linear regression for the mean OIS values is indicated by the bold line. Additional data from cores PC13 (HU90-013-013, square) and MD99-2227 (triangle), both drilled at nearby locations are indicated for comparison. Open symbol: samples from glacial stages; filled symbol: samples from interglacial intervals. Large black circle indicates the position of the modern value measured in a surface sediment sample from box core HU90-013-017. (b) Location of Sm/Nd isotope ratios of the clay-size fraction from Site 646, Leg 105 ODP in regard to the potential regional end members. Due to the scattering of the Sm/Nd ration in a single source, each end member is characterized by a mean and a median value calculated from the literature database. As an exception, the North American Shield end member corresponds to a composite ("Canadian Shield Composite") value proposed by McCulloch and Wasserburg (1978). Mixing calculations are based on three end members: (1) an old craton represent by the North American Shield composition ($^{143}\text{Nd}/^{144}\text{Nd}=0.51105$, $^{147}\text{Sm}/^{144}\text{Nd}=0.095$, $[\text{Nd}]=25$ ppm); (2) a young crust characterized by a Panafrican and/or Variscan ratio from Europe or Greenland ($^{143}\text{Nd}/^{144}\text{Nd}=0.51208$, $^{147}\text{Sm}/^{144}\text{Nd}=0.1145$, $[\text{Nd}]=33$ ppm); (3) a volcanic source defined by a mantel-like isotope signature ($^{143}\text{Nd}/^{144}\text{Nd}=0.51300$, $^{147}\text{Sm}/^{144}\text{Nd}=0.1756$, $[\text{Nd}]=14.5$ ppm). For details and literature references see Innocent et al. (1997) and Fagel et al. (1999). The contribution of the three selected end members is calculated within the triangle indicated on Fig. 5b. Relative contributions reported in Table 1 are indicative ($\pm 10\%$) because of the uncertainty of the end member compositions. Error bars on mean $^{147}\text{Sm}/^{144}\text{Nd}$ (i.e. estimated at $\pm 2\%$) and $^{143}\text{Nd}/^{144}\text{Nd}$ (i.e., $\pm 2\sigma$, data from Table 2) ratios are indicated on a and b.

an effect of glacial enhancement of clay-size particle production through glacial erosion (except for OIS 7). Consequently NAS supplies are higher (relatively to other end-members, but also in absolute terms) during glacial intervals than during interglacials.

To better illustrate the variation of each end-member contribution from one stage to another, the calculated fluxes were normalized to the modern value measured in a surface sediment sample from box core HU90-013-017 (from nearby ODP 646 site; 58°12.51'N, 48°21.6'W; Wu and Hillaire-Marcel, 1994). The representative modern flux was calculated using Sm–Nd data from Innocent et al. (1997) and clay-size fraction data from Fagel et al. (1996). The age of the top 1 cm sample of box core HU90-013-017 was estimated to be at 580 yr (i.e., AMS ¹⁴C age of planktic foraminifera corrected for an apparent surface-water age of 400 years (Wu and Hillaire-Marcel, 1994). This age matched with the age measured on benthic foraminifera tests, suggesting that surface sediment is well preserved at this coring site (Wu and Hillaire-Marcel, 1994). The normalized clay-size fluxes (i.e., sample flux/surface flux) averaged for each OIS range between 0.3 and 1 (Table 2). During glacial intervals, normalized NAS fluxes range from ≤2 in OIS 8 and 10, to 3 in OIS 6, and even 3.8 in OIS 2. Interglacial NAS supplies are lower than modern ones (<0.8), except for one OIS 5 sample (Table 1). NAS supplies are absent in 3 samples from OIS 7. Normalized YC supplies range between 0.1 and 2.

Glacial intervals are usually enriched in YC material (normalized flux > 1), but to a lesser extent in OIS 10 (<1.3). The normalized YC flux is somewhat higher in OIS 7 relative to other interglacials (0.9–1.5; Table 1).

Normalized MAR supplies are low (<1) compared to the present contribution. Ubiquitous in samples older than OIS 6, MAR supplies are occasionally absent in younger samples. Normalized MAR supplies usually vary between 0.1 and 0.3 but exceed a value of 0.3 during most of the OIS 7 and OIS 8 time span (i.e., from ~200 to ~312 kyr), as well as at the base of the studied section (i.e., in OIS 10, >360 kyr). MAR supplies are greater during glacials than during the following interglacials, except for the OIS 6.

4.4. Paleoceanographic implications

At the entrance of the WBUC into the Labrador Sea, off South Greenland, the fine fractions show mean Sm–Nd isotope signatures that are relatively OIS-specific, at least for the last 365 kyr, but generally ¹⁴³Nd/¹⁴⁴Nd and ¹⁴⁷Sm/¹⁴⁴Nd ratios are systematically lower during glacials than during the subsequent interglacials (Fig. 2

and Table 2). At ODP site 984, South of Iceland, a similar Nd isotope shift has been observed for the clay-size fractions, during the OIS 6/5 deglaciation (Bout-Roumazeilles et al., 1998). This shift and the accompanying mineralogical changes were explained by changes in both source provenances and deep currents (Frank et al., 2001). Based on a compilation of data from various North Atlantic sites, Frank et al. (2001) proposed that a reorganisation of deep currents occurred during the OIS 6/5 transition accompanying a northward migration of the sites of NADW formation.

In the Labrador Sea, proximal supplies notably from southern Greenland are characterized by a low Sm/Nd ratio and unradiogenic Nd NAS signature. Distal fine-fraction supplies are carried by deep currents crossing Eastern Irminger and Iceland basins. Distal supplies from the eastern and northeastern Greenland margin, that could have been transported to the study site by the DSW and/or the surface East Greenland Current (Fig. 1) are not necessarily isotopically distinct from sediment transported from Europe and/or Scandinavia by the NEADW. The only distal source with an unequivocally distinct Sm–Nd isotope fingerprint (i.e., higher Sm/Nd ratio mainly inherited from mantle-like MAR source) would be carried by deep currents from the Reykjanes and Iceland areas, with NSOW masses (Fig. 1). The systematic shifts in ¹⁴³Nd/¹⁴⁴Nd ratios (on the order of ~4 εNd; Table 2) during the last four deglaciations could thus be explained by enhanced MAR supplies into the Labrador Sea during interglacials and/or a relative decrease of other, less-radiogenic Nd sources.

The OIS 6/5 deglaciation shift in Nd isotope ratios is less pronounced at ODP site 646 than at the ODP site 984: ~4 εNd vs. ~8 εNd, respectively (Frank et al., 2001). This could be explained by an overall lower sensitivity of fine fractions from the Western North Atlantic to MAR supplies, due to more pronounced proximal NAS supplies. However, at ODP site 646, MAR fluxes do not show any clear glacial/interglacial trend, except a long-term trend decreasing from OIS 10 to OIS 1 (Fig. 5). The relatively steady MAR influx suggests a similarly steady transport from the east throughout most of the interval. In contrast, surface sediments suggest high MAR inputs. Thus, the present deep current conditions appear atypical with respect to the past 365 kyr (0 < present-normalized MAR flux < 0.5; Table 1). A change must have occurred within the last 3.2 kyr (the age of the top ODP 646 sample; Table 1). Indeed, a change in sediment fluxes was previously noted in nearby core MD99-2227 dated at ca. 3.1 kyr. The corresponding large increase of MAR supplies, accompanied by a change in the Pb isotope

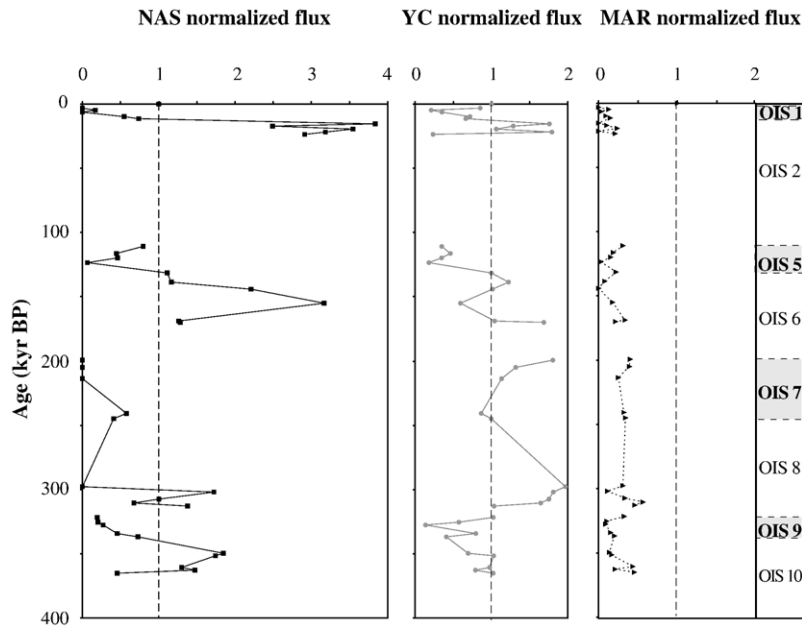


Fig. 5. Estimated contributions of the three identified end member NAS, YC, and MAR for the last four glacial/interglacial cycles. Each end member contribution has been normalized to surface representative sediment signature (vertical dashed line fixed at 1). Data from Table 1. See text for explanation.

ratios, was thought to account for a reduced influence of the DSO, synchronous with full development of the Labrador Sea Water (Fagel et al., 2004).

Over the whole time interval investigated, the fine sediment Sm–Nd ratios in the Labrador Sea seem to have been strongly influenced by continental margin erosional rates. Changes in the absolute NAS flux would fingerprint the intensity of the glacial stages. This is consistent with the atypical mean Sm–Nd signature of OIS8 sediment (i.e., like the interglacial means; Fig. 4a). Low IRD inputs to Rockall Plateau during OIS 8 suggest limited discharge from icebergs, compared to older and younger glaciations (Helmke and Bauch, 2003). Moreover, on a global scale, OIS 8 corresponds to the glacial period with the smallest ice volume of the past 500 kyr, according to the model of Rhohling et al. (1998). Among the four studied interglacials, OIS 7 seems atypical: its fine fraction Sm–Nd signature is marked by no or low (relative and absolute) contributions of NAS (Fig. 4a and Table 1). The unusual characteristics of interglacial OIS 7 was already noted in the North Atlantic area by several authors (e.g., Bauch, 1997; Helmke and Bauch, 2003). For example, on Rockall Plateau in the Iceland Basin (ODP site 980), OIS 9, 5, and 1 are characterized by comparable average benthic foraminiferal $\delta^{18}\text{O}$ values, suggesting residual ice volumes of similar magnitude during each of these warm intervals (Helmke and Bauch, 2003), which

contrasts with OIS 7. On Iceland Plateau North of Iceland, OIS 7 shows only occasional intervals with reduced or no IRD inputs (Helmke and Bauch, 2003). Planktic faunal assemblages of interglacial OIS 7 do not suggest significant warming (Bauch, 1997). OIS 7 follows the atypical glacial stage OIS 8, with low proximal supplies (carrying NAS-like Sm–Nd inputs) suggesting limited ice-margin erosion.

5. Conclusion

The long-term evolution (i.e., over the last 365 kyr) of Sm–Nd ratios of fine particle fractions in deep Labrador Sea sediments reflects changes in source provenance and deep-current paleointensity.

Among the last four interglacials, OIS 9, 5, and 1 display a similar mean Sm–Nd signature in the fine fraction.

Glacial Sm–Nd signatures are characterized by systematically lower $^{143}\text{Nd}/^{144}\text{Nd}$ and $^{147}\text{Sm}/^{144}\text{Nd}$ ratios than interglacials, reflecting enhanced proximal supplies (characterized by NAS-like Nd isotope composition) related to continental margin erosion. The sedimentary Sm–Nd glacial signature can be used as a fingerprint of the local or regional intensity of glacial erosion.

In terms of long-distance transport, the flux of distal fine particles transported by deep water masses from the Iceland Basin–Reykjanes Ridge–Iceland areas did not

change significantly between glacial and interglacials, although an overall long-term reduction seems probable. The ODP646 Sm–Nd record confirms previous observations made from the study of nearby core MD99-2227: the late Holocene (i.e. <3.1 kyr BP), characterized by an increase of MAR supplies, appear to be atypical with respect to the past 365 kyr.

Acknowledgements

The authors acknowledge support from Maryse Henry and Michel Preda, both from GEOTOP, for sub-sampling and sample preparation. J. Stoner (Oregon State University) helped with chronology whereas discussions with C. Innocent (BRGM, France) was especially relevant for mixing calculation. Laboratory expenses at GEOTOP were supported by NSERC-Canada (Discovery grant to C. Hillaire-Marcel, and award to the Climate System History and Dynamics network) as well as by the Canadian Foundation for Climate and Atmospheric Sciences (GR-240).

References

- Aksu, A.E., de Vernal, A., Mudie, P.J., 1989. High resolution foraminifer, palynological and stable isotopic records of Upper Pleistocene sediments from the Labrador Sea: paleoclimatic and paleoceanographic trends. In: Srivastava, S.P., Arthur, M., Clement, B., et al. (Eds.), *Proc. ODP Sci. Results*, 105. Ocean Drilling Program, College Station, TX, pp. 617–652.
- Aksu, A.E., Mudie, P.J., de Vernal, A., Gillespie, H., 1992. Ocean–atmosphere responses to climatic change in the Labrador Sea: Pleistocene plankton and pollen records. *Palaeogeogr. Palaeoclimatol. Palaeoecol.* 92, 121–137.
- Austin, W.E.N., Kroon, D., 2001. Deep sea ventilation of the northeastern Atlantic during the last 15,000 years. *Glob. Planet. Change* 30, 13–31.
- Baldauf, J.G., Clement, B., Aksu, A.E., de Vernal, A., Firth, J., Hall, F., Head, M.J., Jarrard, R., Kaminski, M.A., Lazarus, D., Monjanel, A.L., Berggren, W.A., Gradstein, F., Knuttel, S., Mudie, P., Russell Jr., M.D., 1989. Magnetostratigraphy and biostratigraphic synthesis of ocean drilling Program Leg 105: Labrador Sea and Baffin Bay. In: Srivastava, S.P., Arthur, M., Clement, B., et al. (Eds.), *Proc. ODP Sci. Results*, 105. Ocean Drilling Program, College Station, TX, pp. 935–956.
- Bauch, H.A., 1997. Paleooceanography of the North Atlantic Ocean (68–76°N) during the past 450 kyr deduced from planktic foraminiferal assemblages and stable isotopes. In: Hass, H.C., Kaminski, M.A. (Eds.), *Contributions to the Micropaleontology and Paleooceanography of the Northern North Atlantic*. Grzybowski Found, Krakow, pp. 83–100.
- Bauch, H.A., Erlenkeuser, H.S., Jung, J.A., Thiede, J., 2000. Surface and deep water changes in the subpolar North Atlantic during Termination II and the last interglaciation. *Paleoceanography* 15, 76–84.
- Bauch, H.A., Erlenkeuser, H., Spielhagen, R.F., Struck, U., Matthiesen, J., Thiede, J., Heinemeier, J., 2001. A multiproxy reconstruction of the evolution of deep and surface waters in the subarctic Nordic seas over the last 30,000 yr. *Quat. Sci. Rev.* 20, 659–678.
- Berger, A., 1980. The Milankovitch astronomical theory of paleoclimates. A modern review. *Vistas Astron.* 24, 103–122.
- Bertram, C.J., Elderfield, H., Shackleton, N.J., MacDonald, J.A., 1995. Cadmium/calcium and carbon isotope reconstructions of the glacial northeast Atlantic Ocean. *Paleoceanography* 10, 563–578.
- Bout-Roumzeilles, V., 1995. Relations entre variabilités minéralogiques et climatiques enregistrées dans les sédiments de l'Atlantique Nord depuis les 8 derniers stades glaciaires-interglaciaires, Université de Lille I, unpublished. 180 pp.
- Bout-Roumzeilles, V., Davies, V.G., Labeyrie, L., 1998. Nd–Sr–Pb evidence of glacial–interglacial variations in clay provenance and transport in the North Atlantic Ocean. *Min. Mag.* 62A, 1443–1444.
- Boyle, E., 1995. Last-Glacial-Maximum North Atlantic Deep Water: on, off or somewhere in-between? *Philos. Trans. R. Soc. Lond., A* 348, 243–253.
- Boyle, E.A., Keigwin, L.D., 1982. Deep circulation of the North Atlantic over the Last 200,000 years: geochemical evidence. *Science* 218, 784–787.
- Boyle, E.A., Keigwin, L.D., 1987. North Atlantic thermohaline circulation during the past 20,000 years linked to high-latitude surface temperature. *Nature* 330, 35–40.
- Broecker, W.S., Bond, G., Bonani, G., Wolfli, W., 1990. A salt oscillator in the glacial Atlantic? *Paleoceanography* 5, 469–477.
- Callière, S., Hénin, S., Rautureau, M., 1982. *Minéralogie des argiles. Structures et propriétés physico-chimiques*. Masson, Paris. 184 pp.
- Dia, A., Dupré, B., Allègre, C.J., 1992. Nd isotopes in Indian Ocean used as a tracer of supply to the ocean and circulation paths. *Mar. Geol.* 103, 349–359.
- Dickson, R.R., Brown, J., 1994. The production of North Atlantic Deep Water: sources, rates, and pathways. *J. Geophys. Res.* 99, 12319–12341.
- Duplessy, J.C., Shackleton, N.J., Fairbanks, R.G., Labeyrie, L., Oppo, D., Kallel, N., 1988. Deepwater source variations during the last climatic cycle and their impact on the global deepwater circulation. *Paleoceanography* 3, 343–360.
- Fagel, N., Robert, C., Hillaire-Marcel, C., 1996. Clay mineral signature of the NW Atlantic Boundary Under Current. *Mar. Geol.* 130, 19–28.
- Fagel, N., Hillaire-Marcel, C., Robert, C., 1997. Changes in the Western Boundary Under Current outflow since the Last Glacial Maximum, from smectite/illite ratios in deep Labrador Sea sediments. *Paleoceanography* 12, 79–96.
- Fagel, N., Innocent, C., Stevenson, R.K., Hillaire-Marcel, C., 1999. Deep circulation changes in the Labrador Sea since the Last Glacial Maximum: new constraints from Sm–Nd data on sediments. *Paleoceanography* 14, 777–788.
- Fagel, N., Innocent, C., Gariépy, C., Hillaire-Marcel, C., 2002. Sources of Labrador Sea sediments since the Last Glacial Maximum inferred from Nd–Pb isotopes. *Geochim. Cosmochim. Acta* 66, 2569–2581.
- Fagel, N., Hillaire-Marcel, C., Humblet, M., Brasseur, R., Weis, D., Stevenson, R., 2004. Nd and Pb isotope signatures of the clay-size fraction of Labrador Sea sediments during the Holocene: Implications for the inception of the modern deep circulation pattern. *Paleoceanography* 19, PA3002, doi:10.1029/2003PA000993.
- Faure, G., 1986. *Principles of Isotope Geology*. John Wiley and Sons, New York. 589 pp.

- Frank, M., Davies, G.R., Claude-Ivanaj, C., Hofmann, A.W., 2001. Radiogenic isotopes: new tools help reconstruct paleocean circulation and erosional input, *EOS Trans. Am. Geophys. Union* 82, p. 66, 71.
- Ganopolski, A., Rahmstorf, S., 2001. Rapid changes of glacial climate simulated in a coupled climate model. *Nature* 409, 153–158.
- Goldstein, S.L., O’Nions, R.K., 1981. Nd and Sr isotopic relationships in pelagic clays and ferromanganese deposits. *Nature* 292, 324–327.
- Goldstein, S.J., Jacobsen, S.B., 1987. The Nd and Sr isotopic systematics of river-water dissolved material: implications for the sources of Nd and Sr in seawater. *Chem. Geol.* 66, 2454–2472.
- Grousset, F.E., Biscaye, P.E., Zindler, A., Propero, J., Chester, R., 1988. Neodymium isotopes as tracers in marine sediments and aerosols. *Earth Planet. Sci. Lett.* 87, 367–378.
- Hansen, B., Osterhus, S., 2000. North Atlantic-Nordic Seas exchanges. *Prog. Oceanogr.* 45, 109–208.
- Helmke, J.P., Bauch, H.A., 2003. Comparison of glacial and interglacial conditions between the polar and subpolar North Atlantic region over the last five climatic cycles. *Paleoceanography* 18, doi:10.1029/2002PA000794.
- Hillaire-Marcel, C., Aksu, A., de Vernal, A., Ghaleb, B., 1990. Response of Th/U in deep Labrador Sea sediments (ODP Site 646) to changes in sedimentation rates and paleoproductivities. *Geology* 18, 162–165.
- Hiscott, R.N., Cremer, M., Aksu, A.E., 1989. Evidence from sedimentary structures for processes of sediment transport and deposition during post-Miocene times at Sites 645, 646 and 647, Baffin Bay and Labrador Sea. In: Srivastava, S.P., Arthur, M., Clement, B., et al. (Eds.), *Proc. ODP Sci. Results*, 105. Ocean Drilling Program, College Station, TX, pp. 53–63.
- Innocent, C., Fagel, N., Stevenson, R., Hillaire-Marcel, C., 1997. Nd mixing models and sedimentary fluxes in the North Atlantic Ocean. *Earth Planet. Sci. Lett.* 146, 607–625.
- Innocent, C., Fagel, N., Stevenson, R., 1999. Do leaching experiments in deep-sea clays isolate a seawater component? *Can. J. Earth Sci.* 79, 707–713.
- Kissel, C., Laj, C., Mazaud, A., Dokken, T., 1997. Magnetic anisotropy and environmental changes in two sedimentary cores from the Norwegian Sea and the North Atlantic. *Earth Planet. Sci. Lett.* 164, 617–626.
- Kösters, F., Käse, R., Fleming, K., Wolf, D., 2004. Denmark Strait Overflow for Last Glacial Maximum to Holocene conditions. *Paleoceanography* 19, 2019, doi:10.1029/2003PA000972.
- Lassen, S., Kuijpers, A., Kunzendorf, H., Lindgren, H., Heinemeier, J., Jansen, E., Knudsen, K.L., 2002. Intermediate water signal leads surface water response during Northeast Atlantic deglaciation. *Glob. Planet. Change* 32, 111–125.
- Ledbetter, M.T., Balsam, W.M., 1985. Paleoceanography of the deep Western Boundary Under Current on the North American continental margin for the past 25000 yr. *Geology* 13, 181–184.
- Lucotte, M., Hillaire-Marcel, C., 1994. Identification des masses d’eau dans les mers du Labrador et d’Irvinger. *Can. J. Earth Sci.* 31, 5–13.
- McCartney, M.S., 1992. Recirculating components to the deep boundary current of the northern North Atlantic. *Prog. Oceanogr.* 29, 283–383.
- McCave, I.N., Manighetti, B., Beveridge, N.A.S., 1995. Circulation in the glacial North Atlantic inferred from grain-size measurements. *Nature* 374, 149–151.
- McCulloch, M.T., Wasserburg, G.J., 1978. Sm–Nd and Rb–Sr chronology of continental crust formation. *Science* 200, 1003–1011.
- Millo, C., Sarnthein, M., Erlenkeuser, H., Grootes, P., 2003. Last Glacial to Interglacial Variability of the Denmark Strait Overflow. EGS, Nice.
- Moore, D.M., Reynolds, R.C., 1989. *X-ray Diffraction and the Identification and Analysis of Clay Minerals*. Oxford Univ. Press, New York. 332 pp.
- Moros, M., Ender, R., Lackschewitz, K.S., Wallrabe-Adams, H.-J., Mienert, J., Lemke, W., 1997. Physical properties of Reykjanes Ridge sediments and their linkage to high-resolution Greenland Ice Sheet Project 2 ice core data. *Paleoceanography* 12, 687–695, doi:10.1029/97PA02030.
- Oppo, D.W., Fairbanks, R.G., 1987. Variability in the deep and intermediate water circulation of the Atlantic Ocean: Northern Hemisphere modulation of the Southern Ocean. *Earth Planet. Sci. Lett.* 86, 1–15.
- Rahmstorf, S., Alley, R., 2002. Stochastic resonance in glacial climate. *EOS Trans. Am. Geophys. Union* 83, 129, 135.
- Raymo, M.E., Oppo, D.W., Flower, B.P., Hodell, D.A., McManus, J.F., Venz, K.A., Kleiven, K.F., McIntyre, K., 2004. Stability of North Atlantic water masses in face of pronounced climate variability during the Pleistocene. *Paleoceanography* 19, 2008, doi:10.1029/2003PA000921.
- Revel, M., Cremer, M., Grousset, F.E., Labeyrie, L., 1996. Grain-size and Sr–Nd isotopes as tracer of paleo-bottom current strength, Northeast Atlantic Ocean. *Mar. Geol.* 131, 233–249.
- Rholing, E.J., Fenton, M., Jorissen, F.J., Bertrand, P., Gansen, G., Caulet, J.P., 1998. Magnitudes of sea-level lowstands of the past 500,000 yrs. *Nature* 394, 162–165.
- Sarnthein, M., Altenbach, A.V., 1995. Late quaternary changes in surface water and deep water masses of the Nordic Seas and North Atlantic: a review. *Geol. Rundsch.* 84, 89–107.
- Sarnthein, M., Winn, K., Jung, S.J.S., Duplessy, J.C., Labeyrie, L., Erlenkeuser, H., Ganssen, G., 1994. Changes in east Atlantic deepwater circulation over the last 30,000 years: Eight time slice reconstructions. *Paleoceanography* 9, 209–267.
- Schmitz, W.J.J., Mc Cartney, M.S., 1993. On the North Atlantic circulation. *Rev. Geophys.* 31, 29–49.
- Schonfeld, J., Zahn, R., de Abreu, L., 2003. Surface and deep water response to rapid climate changes at the Western Iberian margin. *Glob. Planet. Change* 36, 237–264.
- Shackleton, N.J., Imbrie, J., Hall, M.A., 1983. Oxygen and carbon isotope record of the East Pacific core V19-30: implications for the formation of deep water in the late Pleistocene North Atlantic. *Earth Planet. Sci. Lett.* 65, 233–244.
- Snowball, I., Moros, M., 2003. Saw-tooth pattern of North Atlantic current speed during Dansgaard-Oeschger cycles revealed by the magnetic grain size of Reykjanes Ridge sediments at 59°N. *Paleoceanography* 18, doi:10.1029/2001PA000732.
- Srivastava, S.P., Arthur, M., et al., 1987. *Proc. ODP, Init. Rep.*, 105. Ocean Drilling Program, College Station, TX.
- St. John, K., Flower, B.P., Krissek, L., 2004. Evolution of iceberg melting, biological productivity and the record of Icelandic volcanism in the Irvinger basin since 630 ka. *Mar. Geol.* 212, 133–152.
- Wu, G., Hillaire-Marcel, C., 1994. Accelerator mass spectrometry radiocarbon stratigraphies in deep Labrador Sea cores: Paleoceanographic implications. *Can. J. Earth Sci.* 31, 38–47.